



## Evaluating simulated visible greenness in urban landscapes: An examination of a midsize U.S. city

Jingjing Yan<sup>a</sup>, Reza Naghedhi<sup>a</sup>, Xiao Huang<sup>a,e,\*</sup>, Siqin Wang<sup>b</sup>, Junyu Lu<sup>c</sup>, Yang Xu<sup>d</sup>

<sup>a</sup> Department of Geosciences, University of Arkansas, Fayetteville, AR, USA

<sup>b</sup> Graduate School of Interdisciplinary Information Studies, University of Tokyo, Tokyo, Japan

<sup>c</sup> School of Community Resources and Development, Arizona State University, Phoenix, AZ, USA

<sup>d</sup> Department of Land Surveying and Geo-Informatics, The Hong Kong Polytechnic University, Hung Hom, Hong Kong, China

<sup>e</sup> Department of Environmental Sciences, Emory University, Atlanta, GA, USA

### ARTICLE INFO

Handling Editor: Dr Cecil Konijnendijk van den Bosch

#### Keywords:

Visible greenness  
Green space  
360-degree panoramas  
3D urban analysis  
DeeplabV2 neural network

### ABSTRACT

Urban greenness is critical in evaluating urban environmental and living conditions, significantly affecting human well-being and house prices. Unfortunately, satellite imagery from a bird-eye view does not fully capture urban greenness from a human-centered perspective, while human-perceived greenness from street-view images heavily relies on road networks and vehicle accessibility. In recent years, scholars started to explore greenness measurements from a simulative perspective, among which the simulation of the Viewshed Greenness Visibility Index (VGVI) received wide attention. However, the simulated VGVI lacks a comprehensive assessment. To fill this gap, we designed a field experiment in Fayetteville, Arkansas, by collecting 360-degree panoramas in different local climate zones. Further, we segmented these panoramas via the state-of-the-art DeeplabV2 neural network to obtain the Panoramic Greenness Visibility Index (PGVI), which served as the ground-truthing human-perceived greenness. We assessed the performance of VGVI by comparing it with PGVI calculated from field-collected panoramas. The results showed that, despite the disparity of performance in different local climate zones, VGVI highly correlates to the PGVI, indicating its great potential for various domains that favor urban human-perceived greenness exposure.

### 1. Introduction

Urbanization has accelerated globally since the beginning of the 21st century. In 2021, 57 % of the world's population was inhabiting urban areas, while the percentage for North America was much higher, nearly reaching 75 % (World Bank, n.d.). The rapid growth of the urban population accelerated the expansion of the urban and metropolitan areas, leading to a big challenge for urban planning and management, especially for the maintenance and development of greenspace (Haaland and van den Bosch, 2015; Muhamad Nor et al., 2021; Wei et al., 2022).

Urban greenness (i.e., vegetation) is an essential criterion for evaluating the living environment in various aspects of urban life. From an environmental point of view, urban greenness plays a vital role in absorbing air pollution (Currie and Bass, 2008), relieving the urban heat island effect (Gunawardena et al., 2017; Qiu et al., 2013), and reducing noise (Dzhambov and Dimitrova, 2014). In addition to its environmental effects, urban greenness has economic influences in cities and affects

housing prices and city attractions. Previous studies showed that appealing urban greenness caused positive implications on nearby house prices by providing attractive amenities (Daams et al., 2019) and contributing to higher life satisfaction for residents (Gintoli et al., 2020; Wu et al., 2022). Furthermore, unevenly distributed urban greenness can be closely related to race and ethnicity issues (Heynen et al., 2006) that certain racial/ethnic minorities and disadvantaged groups (e.g., lower income) have access to fewer greenspace (Boone et al., 2009), which deserves stakeholders' attention and more consolidative sustainability strategies to improve the quality of community (Wolch et al., 2014).

Urban greenness is also considered to be crucial for human health. Yuan et al. (2021) utilized a meta-analysis involving eight studies and concluded that the greater exposure to urban greenness leads to a lower risk of mortality by cardiovascular diseases. Similar outcomes were also demonstrated by Kondo et al. (2018) and Twohig-Bennett & Jones (2018). In addition, living in a greener place also benefits blood

\* Corresponding author at: Department of Geosciences, University of Arkansas, Fayetteville, AR, USA.

E-mail addresses: [xh010@uark.edu](mailto:xh010@uark.edu), [xiao.huang2@emory.edu](mailto:xiao.huang2@emory.edu) (X. Huang).

pressure, blood glucose, body mass, and even low birth weight (Yang et al., 2021a). Shin et al. (2020) showed that enhanced exposure to urban greenness could reduce anxiety and sleep disorders by opposing computer screen use for long hours. Besides, urban greenness can inspire people to do more physical activities. Research indicated that more exposure to urban greenness in the community could result in more outdoor activities in all age groups, including children (Lambert et al., 2019), adults (Lambert et al., 2019; Thomsen et al., 2018), and elderly groups (de Keijzer et al., 2020).

The assessment of urban greenness has seen significant improvement. In the early days, most assessing methods were based on satellite-based imagery from a bird-view perspective (Bai et al., 2022; Franco and Macdonald, 2018; Qian et al., 2015). Satellite imagery brings an overview of spatial distribution of green and non-green space, which can help estimate the macroscopical environmental effect of urban greenness, however, it cannot provide detailed guidance for assessing housing prices or human health enhancement because it fails to reflect the greenness from a human-eye aspect (Labib et al., 2021). How to derive visible greenness from the human eye has become a hot research topic.

With the development of street view images, recent studies proposed photo-based urban greenness assessment from a profile view by extracting the greenness level from street view images (Biljecki and Ito, 2021; Dong et al., 2018; Hu et al., 2021; Li et al., 2015; Li and Ratti, 2018; Lu, 2019). However, photo-based urban greenness is only accessible where street-view vehicles are reachable (Labib et al., 2021). Simulated urban greenness, a geospatial data-based method to calculate greenness, can overcome such challenges (Brinkmann et al., 2022; Labib et al., 2020, 2021). The geospatial datasets are commonly used geospatial data generated from unmanned aerial vehicle mapping systems. The computational representation of urban green spaces emulates the human perspective within a three-dimensional environment, offering comprehensive coverage. This digital approximation has the potential to supply highly detailed distributions of green spaces, thus providing invaluable data for urban planning and ecological analysis (Brinkmann et al., 2022; Wang et al., 2019; Yu et al., 2016). However, the lack of comprehensive evaluation of the simulated urban greenness hinders its applications, especially the assessment in different urban settings. As proposed by Labib et al. (2021), an extensive empirical validation involving large-scale ground truthing would significantly enhance the reliability and applicability of the simulated greenness visibility model. The development of a high-resolution, eye-level urban greenness distribution with comprehensive coverage is pivotal in formulating more insightful recommendations for urban planning and public health initiatives. Consequently, there is an immediate necessity to utilize a standardized and rigorously verified methodology for the evaluation of urban greenness.

In this study, we aim to conduct a comprehensive evaluation of the simulated urban greenness and investigate its adaptation under different Local Climate Zones (LCZs), proposed by Demuzere et al. (2022), as a widely used categorization of urban environments. To achieve these objectives, we applied a recently proposed simulation of the viewshed greenness visibility index (VGVI) to our study site, i.e., Fayetteville, Arkansas in the United States of America (U.S.). This index adopted both viewshed analysis and distant decay function (Labib et al., 2021), which has brought wide attention but has not been comprehensively assessed. We collected panoramas within complex urban settings to derive a panoramic greenness visibility index (PGVI), and further used the PGVI as the ground truth to evaluate the performance of VGVI. The particular contributions of this work are summarized as follows:

- 1) We calculated the VGVI of Fayetteville at the fine-grained level (one-meter resolution) from the human-eye level using open-sourced geospatial data, i.e., Lidar point cloud, satellite-based earth observation, and building footprints.
- 2) We considered different urban settings based on the new concept of LCZs to collect 858 panoramic photos in the field experiment based

on both vehicle-reachable and walk-reachable locations. Then, we calculated the PGVI in the collected panoramas by a state-of-the-art segmentation method, i.e., Deeplabv2 (Cheng et al., 2020).

- 3) We assessed the VGVI by comparing it with the PGVI. In particular, we detailed the evaluation in different LCZs and explored the universality of VGVI under various urban settings.
- 4) We discussed the importance and current challenges of the simulation of VGVI and proposed its potential applications.

## 2. Background

### 2.1. From bird-view to street-view greenness

Remote Sensing is a commonly used technique to assess and map urban greenness (Yin et al., 2021). Although quantifying urban greenness with high-resolution data (Franco and Macdonald, 2018; Qian et al., 2015) or enhanced computational neural networks (Bai et al., 2022) were proposed in recent years, some shrubs and lawns covered by canopy are still hard to be detected. Besides, remote sensing measurements have their inherent limitation in that only the bird's view from top-down sensors is available, which leads to missing information such as the layout and height of urban buildings. Yang et al. (2009) showed that the greenness observed in a human view depends on the arrangement of buildings and roads. Through a thorough analysis, Jiang et al. (2017) discovered that the urban greenness derived from aerial tree cover density was inconsistent with the urban greenness derived at a human eye level. Those studies emphasized the importance of eye and site visits to measure urban greenness.

Thus, quantifying urban greenness from a profile view is more relevant to human's actual perception of greenness. Meitner (2004) designed questionnaires to rate urban greenness access from human perception. However, those questionnaires provided a limited understanding and were constrained to uncertain response criteria. Yang et al. (2009) manually extracted the green pixels from four-direction color photos captured at a ground location to develop a green view index. However, this method is time-consuming and labor consuming. Inspired by extracting the green pixels from the color photos, Li et al. (2015) modified the green view index to extract the green vegetation pixels from google street view images and proposed the street-view green view index by separating the 360-degree panoramic street-view images into six directions horizontally and three view angles vertically. Larkin & Hystad (2018) stated that the techniques of the street-view green view index provided specific knowledge about urban greenness exposures. In recent years, the street-view green view index has developed as a state-of-the-art methodology to assess urban greenness (Chen et al., 2020; Dong et al., 2018; Xia et al., 2021; Zhang et al., 2021) and has been applied in different domains, such as human activities (Larkin and Hystad, 2019; Lu, 2019), socioeconomic conditions (Wang et al., 2021) and house price models (Yang et al., 2021a).

### 2.2. A new human-view frontier: simulation of visible greenness

Although the street-view green view index brings some new horizons, a significant limitation is that the availability of street-view images depends on road networks and vehicle accessibility (Rzotkiewicz et al., 2018). Moreover, the images of big cities are updated more frequently than the images of small towns. Therefore, a reliable approach is still needed to estimate community-level greenness in a robust and timely manner (Labib et al., 2020).

Several studies have started to explore the simulated urban greenness from the human eye level to issue the limitations of the street-view green view index. Viewshed analysis, defined as a geographical area visible from a location, has been used to assess the landscape visibility in different aspects, such as the aesthetic potential of the landscape (Sahraoui et al., 2016) and urban design evaluation (Yang et al., 2007). Tabrizian et al. (2020) calculated the viewshed of foliage to provide

suggestions for urban greenness planning. Nutsford et al. (2015) considered the vertical degrees of visibility to adjust the standard ground-level viewshed to an eye-level viewshed. Such simulations of urban greenness are not constrained to specific locations and are suitable to measure urban greenness at a community level (Labib et al., 2020; Labib et al., 2021). Besides, the viewshed analysis was also used at viewpoints of different floors to estimate urban greenness in a three-dimensional (3D) central business district (Wang et al., 2019; Yu et al., 2016). However, these analyses require the setting of observation points or platforms according to the 3D building morphology, posing challenges to its applicability. In addition, the perspective effect of the human eye allows the eye to perceive a more considerable prominence (Chen et al., 2015; Kumsap et al., 2007) and capture more information (Bishop, 2016; Kumsap et al., 2007) from near objects. Built upon the previous studies, Labib et al. (2021) developed a new integrated simulation of VGVI to assess urban greenness, which gained wide attention. In the simulation of VGVI, not only the viewshed analysis was applied, but a distant decay function was also incorporated to simulate the effect of the human eye perception discrepancy within various distances. In sum, the simulation of VGVI provides a new frontier for assessing urban greenness, and we choose the VGVI as our main focus to evaluate its accuracy.

### 2.3. The promising of VGVI

Viewshed of urban greenness includes all vegetational points in the line-of-sight at a given site and eliminates all the other points beyond the ground or blocked by terrain and buildings (Wang et al., 2019; Yu et al., 2016). Fig. 1 presents the concept of VGVI. From the reader's perspective (an angle of a high squint), a sizeable green area can be observed, including the trees and shrubs both on the sidewalk and behind the buildings. In contrast, assuming the observer stands at the pedestrian crossing, only green belts (i.e., the grass and trees) on both sides of the road are visible to the observer. The green space behind the buildings is invisible to this observer due to sight blocking. Therefore, the visible greenness in certain locations is less than expected, although the neighborhood is within a green area (Labib et al., 2021).

VGVI implemented Bresenham's algorithm (Bresenham, 2010) to launch the line-of-sight. The viewshed analysis for a given observer spot generated a binary matrix indicating which cells are visible to the observer. Based on experimentation and expert opinions, a distant decay function was applied to mitigate the bias caused by the effect of the decrease in perceived prominence of features with growing observer distance (Labib et al., 2021).

The inputs of VGVI simulation include the digital surface model (DSM) dataset, the digital terrain model (DEM), and the green or non-green space. These inputs are relatively easy to attain on a global scale or a local scale with a finer resolution, showing the considerable potential of its application on large-scale urban greenness assessment. However, the performance of VGVI has not been thoroughly tested, especially in the different urban types. Therefore, in this study, we designed a field experiment to evaluate the validity of VGVI.

## 3. Methods and materials

### 3.1. Case study area

We selected Fayetteville to collect the ground-truth 360-degree panoramas by a field experiment to compute the PGVI and further calibrate the VGVI. Fayetteville is the second-biggest city in Arkansas, U. S. (Fig. 2a). Based on the US Census data (Census, 2021), the city has a total population of 95,230 and a total area of 143 km<sup>2</sup>. Fayetteville exemplifies a substantial number of mid-sized cities in the United States, making it an ideal case study for our research. Its selection as our investigation site facilitates a thorough and significant evaluation, thereby yielding robust and transferrable insights. We hypothesized that VGVI might perform differently in different land use and land cover, and thus we evaluated the performance of VGVI to measure greenness in Fayetteville in different Local Climate Zones (LCZs). Demuzere et al. (2022) released a global map of LCZs to assist the urban-scale environmental science and analysis. LCZs reflect the association between urban land cover and land use. The map generally comprises ten built types and seven natural land cover types (Table 1).

In this study, LCZs were scaled to Fayetteville (Fig. 2b), which includes five built types (i.e., compact lowrise, open midrise, open lowrise, large lowrise, and sparsely built) and five natural land cover types (i.e., dense trees, scattered trees, low plants, bare soil or sand, and water). Corresponding with the original LCZ index, the five built types of compact lowrise, open midrise, open lowrise, large lowrise, and sparsely built are named LCZ 3, 5, 6, 8, and 9, respectively. The dense trees, scattered trees, low plants, bare soil or sand, and water correspond to LCZ 11, 12, 14, 16, and 17, respectively (Table 1).

### 3.2. Experimental design

To assess the performance of VGVI, we designed a field experiment to collect the 360-degree panoramas and further compute the Panoramic Greenness Visibility Index (PGVI) from these panoramas, especially for those locations that are not vehicle-accessible. The sample collecting date happened in the green season of Fayetteville, mainly in the summer of 2022. The PGVI served as the ground-truthing eye-level greenness in Fayetteville. Fig. 3 presents the workflow of our experiment. We introduce essential steps in the following subsections.

#### 3.2.1. Sampling equipment

We used the Ricoh Theta V 360 camera, a camera that captures 360-degree panoramas with a resolution of 5.5k. The advantage of this camera is that once 360-degree photos are captured, well-stitched panoramic images can be generated in its default mobile phone application. Although this camera has a built-in Global Positioning System, higher positional accuracy is preferred. Therefore, we used the Qstarz BT-Q1000XT GPS Receiver, which ensures accuracy within 3 m, to record the precise location of each panorama. We also applied a tripod to stabilize the camera while holding the camera at the height of eye level (1.7 m).



Fig. 1. Conceptual display of Viewshed Greenness Visibility Index (VGVI).

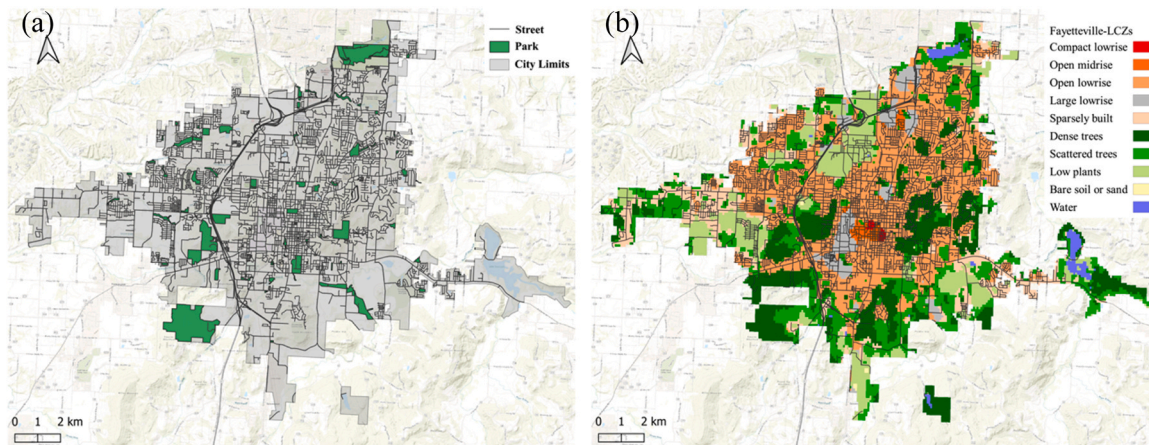


Fig. 2. (a) Study area city of Fayetteville (data Source: City of Fayetteville (n.d.)), (b) LCZs distribution of Fayetteville.

Table 1

The summary of Local Climate Zones (Demuzere et al., 2022). Check marks in the table mean these LCZ types are available in Fayetteville; cross marks mean otherwise.

Climate zone types	LCZ number	Meaning	Definition	Fayetteville
Built land cover types	1	Compact highrise	Dense mix of tall buildings to tens of stories	×
	2	Compact midrise	Dense mix of midrise buildings (3–9 stories)	×
	3	Compact lowrise	Dense mix of lowrise buildings (1–3 stories)	✓
	4	Open highrise	Open arrangement of tall buildings to tens of stories	×
	5	Open midrise	Open arrangement of midrise buildings (3–9 stories)	✓
	6	Open lowrise	Open arrangement of lowrise buildings (1–3 stories)	✓
	7	Lightweight lowrise	Dense mix of single-story buildings	×
	8	Large lowrise	Open arrangement of large lowrise buildings (1–3 stories)	✓
	9	Sparsely built	Sparse arrangement of small or medium-sized buildings in a natural setting	✓
	10	Heavy industry	Lowrise and midrise industrial structures (towers, tanks, stacks)	×
Natural land cover types	11	Dense trees	Heavily wooded landscape of deciduous and/or evergreen trees	✓
	12	Scattered trees	Lightly wooded landscape of deciduous and/or evergreen trees	✓
	13	Bush, scrub	Open arrangement of bushed, shrubs, and short, woody trees	×
	14	Low plants	Featureless landscape of grass or herbaceous plants/crops	✓
	15	Bare rock or paved	Featureless landscape of rock or paved cover	×
	16	Bare soil or sand	Featureless landscape of soil or sand cover	✓
	17	water	Large, open water bodies such as seas and lakes	✓

### 3.2.2. Sampling protocols

The sample sites were randomly selected within each LCZ in our study area. Water bodies were ignored for site selections, given that water bodies are not usually accessible to humans. Besides, only a few pixels in our area contain the LCZ of bare soil or sand; thus, no random sample points were allocated to such types of LCZs. So, eight LCZ types were considered in our study. The detailed procedure of the panorama collection is described below:

- (1) Identifying the area for each type of LCZ in Fayetteville (a total of eight LCZ types)
- (2) Creating 100 random sampling points along the street for each LCZ (a total of 800 locations)
- (3) Collecting panorama for each random pointed location or its near location for convenience and safety
- (4) Geotagging the panoramas and importing them to Google MyMap for documentation (shorturl.at/LRV29)

Although sampling locations are randomly generated along the street network, our methodology prioritizes safety by ensuring data collection occurs on the sidewalk when the sampling point is positioned on a main road. Furthermore, our sampling design strategically encompasses a multitude of samples within internal communities, areas often overlooked by street-view vehicles due to the smaller scale of these roads. Fig. 4 presents the spatial distribution of sample sites. Since the open lowrise climate zone is scattered throughout the city when we tried to collect the samples in other LCZs, some samples were not easily reachable, so we chose a nearby location to collect the data for convenience. Thus, several samples from other LCZs fell into the open lowrise climate zone, resulting in 158 samples for this LCZ. A total of 858 panoramas were eventually obtained in our experiment.

### 3.2.3. Calculation of PGVI from greenness segmentation

Extracting the green pixels from a panorama is a precondition for generating quantitative information about vegetation. In this study, we applied a pre-trained DeepLab2 model (Cordts et al., 2016) to extract the urban greenness from the panoramas. After obtaining the pixel-based feature map, the non-vegetation category in the semantic labels was removed, and PVGI can be calculated as the following:

$$PVGI_{deeplab2} = \frac{NoP_{veg}}{NoP_{total}} \quad (1)$$

where  $NoP_{veg}$  is the number of vegetation pixels and the  $NoP_{total}$  is the total number of pixels in the panoramas.

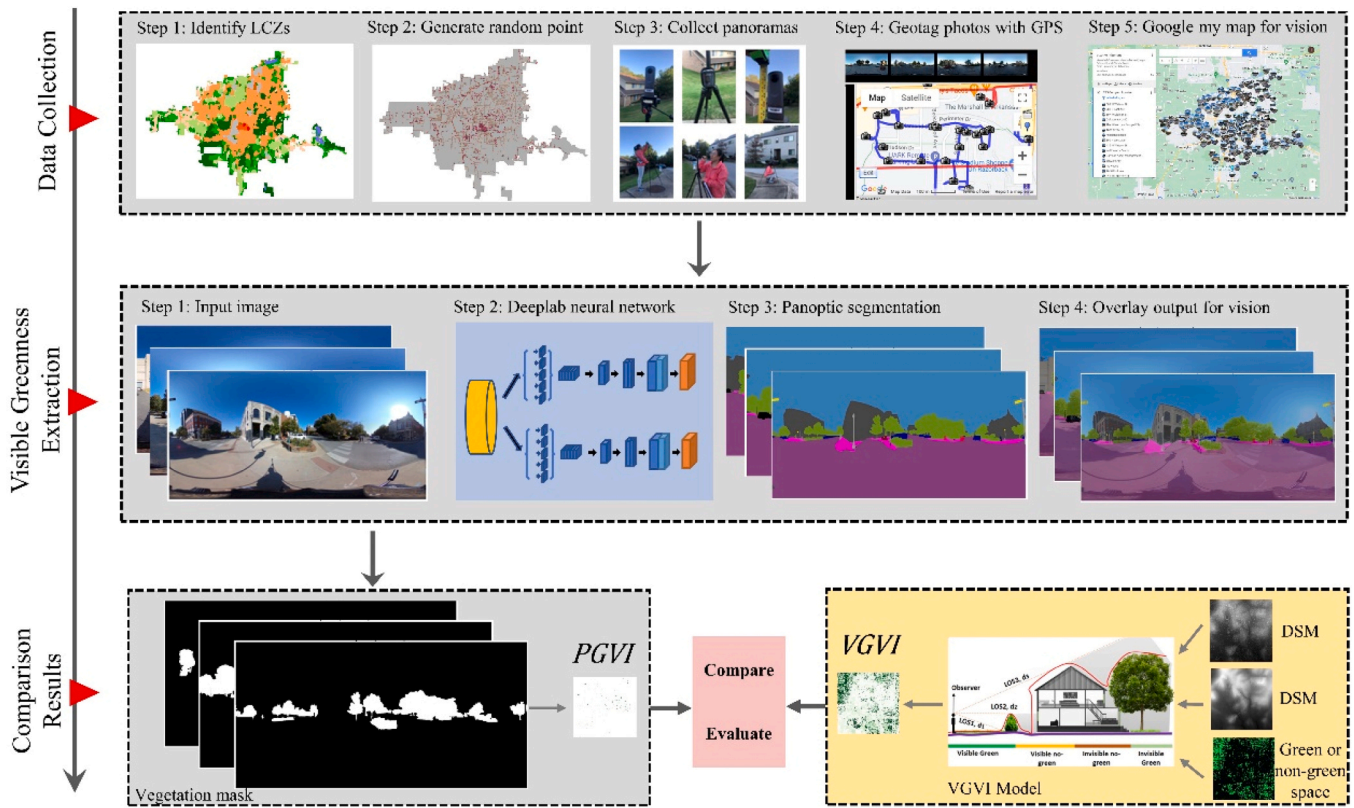


Fig. 3. Experimental workflow of this study.

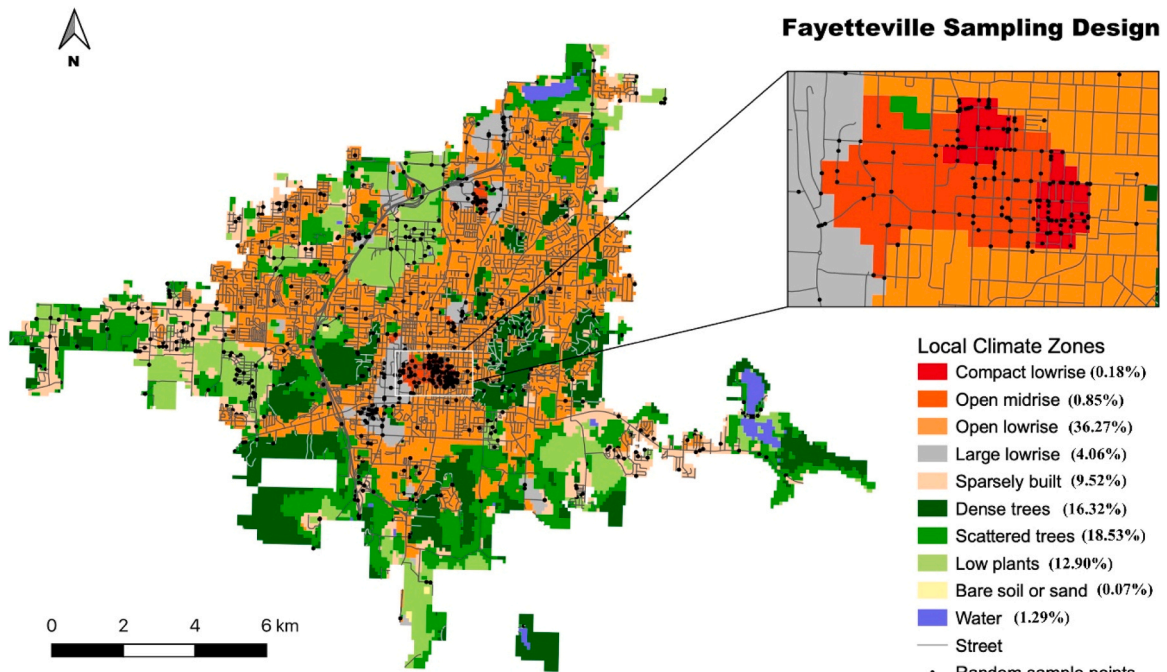


Fig. 4. Spatial distribution of the sampling sites and the local climate zones (LCZs) in Fayetteville, Arkansas.

### 3.3. VGVI Calculation

To set the eye-level view aspect, we considered a modified observer height of 1.7 m at a given location to launch the LOS and set the maximum view distance as 550 m based on the method from Labib et al. (2021). DSM and DEM are derived from LiDAR and provided by US

Geological Survey (Dollison and Maxwell, 2019). Green and non-green space datasets show whether a specific location in a study area belongs to vegetation or non-vegetation. Following the early study (Braun and Herold, 2004), we calculated green and non-green spaces from high-resolution normalized difference vegetation index (NDVI) derived from the National Agriculture Imagery Program (NAIP) in the growing

season of 2022. The building footprints of Fayetteville, based on the remote sensing imageries from 2019 to 2020 licensed by Microsoft, were used to mask the building locations, as in our model, the observers are not allowed to stand on the top of buildings.

According to Labib et al. (2021), viewshed analysis and distant decay served as the main component parts of VGVI modeling. For any given observer spot, a matrix of visibilities that depicts visible information is generated through the viewshed analysis, and a matrix of weights is generated through the distant decay function. The products of these two matrixes of visibilities and weights contribute to the VGVI. The mathematical formation of VGVI follows:

$$VGVI_j = \frac{\sum_{p=1}^n G_{pj} \times df_{pj}}{(\sum_{p=1}^n G_{pj} \times df_{pj}) + (\sum_{q=1}^m V_{qj} \times df_{qj})} \quad (2)$$

where  $VGVI_j$  is the greenness visible index value at any observer location  $j$ ;  $p$  represents the  $p$ th visible green cell for the observer location;  $q$  represents the  $q$ th visible non-green cell for the observer location;  $n$  and  $m$ , respectively, represent the total number of visible green and non-green cells.  $G_{pj}$  is the  $p$ th visible green cell,  $V_{qj}$  is the  $q$ th visible non-green cell, and  $df_{pj}$  stands for the pre-calculated weights by distance decay function at the  $p$ th visible green cell for observer location  $j$ . Similarly,  $df_{qj}$  represents the weights at the  $q$ th visible non-green cell. Thus, the VGVI, ranging from 0 to 1, represents the proportion of the visible green cells over the total visible cells.

### 3.4. Evaluation of VGVI

In this study, we compared the distribution pattern of VGVI and bird-eye greenness (i.e., green and non-green spaces) derived from NDVI (bird-view) in Fayetteville to explore how bird-eye greenness is different from human-eye greenness. Moreover, we also explore the correlation between field-collected PGVI and simulated VGVI, aiming to shed light on the performance of VGVI. In view of the pair-wise relationship between PGVI and VGVI, we have additionally employed the Two One-Sided Test (TOST), a paired equivalence test designed to validate the statistical significance of their similarity, as proposed by Williams (1959). We adopted a 0.01 significance level for all subsequent statistical evaluations to ensure rigorous examination.

The TOST procedure involves a modification of the conventional two-sided Student's t-test by reversing the roles of the null and alternative hypotheses (Mara and Cribbie, 2012). In the TOST procedure, if  $\theta$  represents the margin of equivalence, the null hypothesis asserts that the population mean difference score ( $\mu_1 - \mu_2$ ) falls outside a predefined equivalence interval ( $H_{01} : \mu_1 - \mu_2 \geq \theta$  or  $H_{02} : \mu_1 - \mu_2 \leq -\theta$ ), suggesting that the two groups or conditions are considered non-equivalent. Consequently, the alternative hypothesis asserts that the mean difference score is sufficiently small to be within the determined equivalence interval, suggesting that the population means are indeed equivalent ( $H_1 : -\theta < \mu_1 - \mu_2 \leq \theta$ ). The null hypothesis is characterized by two simultaneous predictions, both of which must be rejected to conclude that the mean differences in paired observations are equivalent.  $H_{01}$  would be rejected if  $t_1 \geq -t_{\alpha, n-1}$  and  $H_{02}$  would be rejected if  $t_2 \geq -t_{1-\alpha, n-1}$ :

$$t_1 = \frac{\bar{x}_1 - \bar{x}_2 - \theta}{S_{diff} / \sqrt{n-1}} \text{ and } t_2 = \frac{\bar{x}_1 - \bar{x}_2 - (-\theta)}{S_{diff} / \sqrt{n-1}} \quad (3)$$

where  $\bar{x}_1$  and  $\bar{x}_2$  are the sample means, the  $S_{diff}$  is the standard deviation of the difference scores, and  $n$  is sample size.

## 4. Results

### 4.1. Greenness segmentation from panoramas

Fig. 5 presents the PGVI calculated from the greenness extraction with different green tones of dots. The average PGVI for all the sampling points is 0.13, meaning the average greenness derived from the panoramas is 13 %. The area with more dense buildings, such as the downtown and the University of Arkansas, exhibits a lighter green tone than the suburban area, indicating their lower visible greenness. The building acts as a major factor that obstructs sight (Biljecki and Ito, 2021). The histograms in Fig. 5 show the distribution of PGVI in each LCZ. In general, LCZ 11 (i.e., dense tree), shows a relatively higher greenness level with an average PGVI of 0.293, and LCZ 14 (i.e., low plants), shows a lower greenness level with an average PGVI of 0.058. For the built types (i.e., LCZ3–9), the PGVI is around 0.1.

Fig. 6 presents five selected cases. From the scope view listed on the right of the PGVI distribution map, the locations (a)–(e) represent LCZ 8,

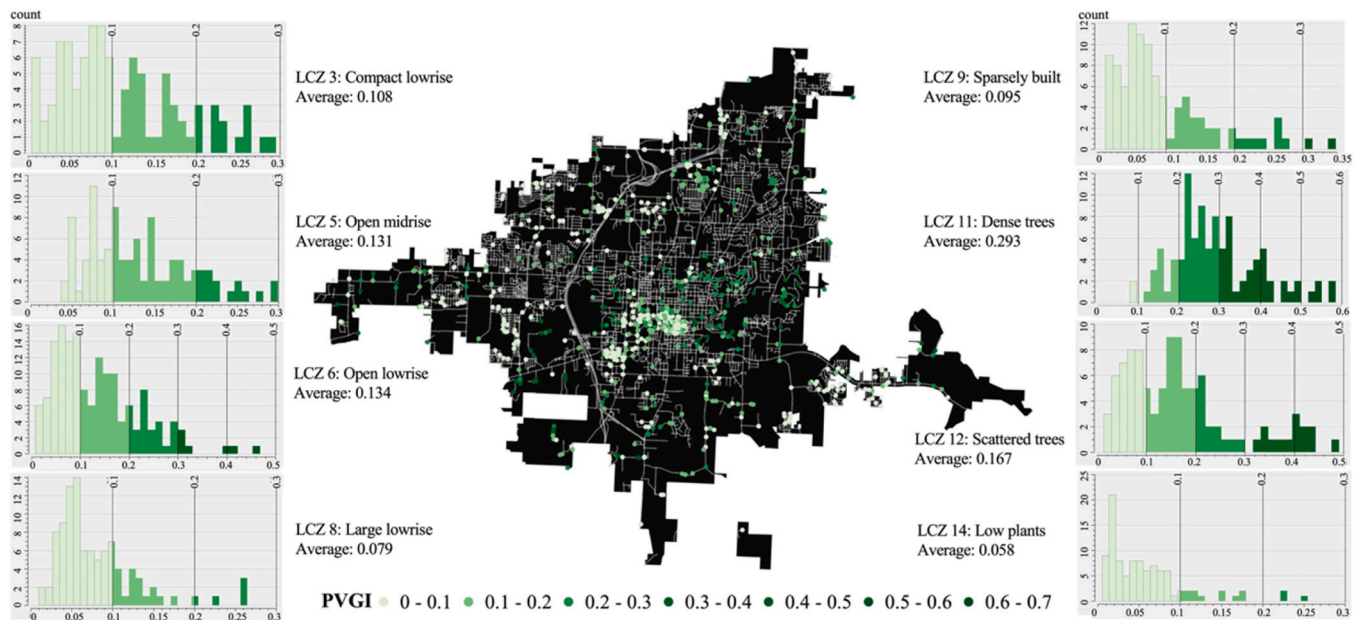


Fig. 5. The PGVI distribution from collected panoramas in our study area via Deeplabv2 segmentation. In the histograms, the x-axis denotes PGVI, and the y-axis denotes the count of samples.

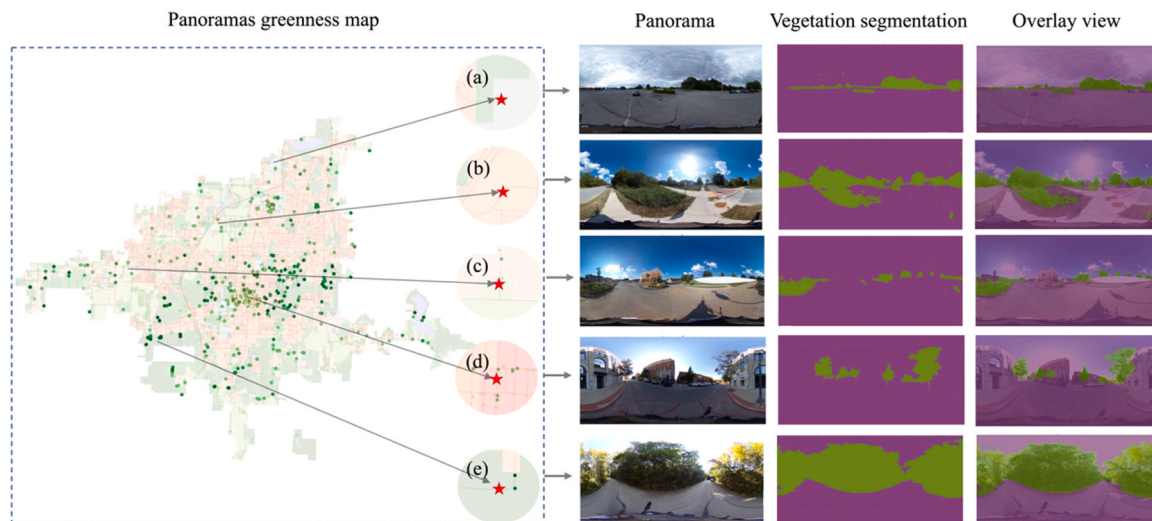


Fig. 6. Selected five cases, i.e., (a)-(e), of panoramic greenness segmentation from panoramas. The red stars represent the sample locations of these five cases. The overlay views represent the overlay of vegetation segmentations (with 60 % transparency) on panoramas.

LCZ 9, LCZ 14, LCZ 3, and LCZ 11, respectively. From case (a) in LCZ 8 (i.e., large lowrise zone), the pavement occupies an extensive area of the panoramas, which reduces the visible greenness and leads to the lowest average PGVI of LCZ 8 within the five built types. Case (b) in LCZ 9 shows the segmentation result at a location on a sidewalk. We observe that the segmentation for trees and shrubs outperforms the segmentation of grass, especially for the areas where the grass presents a yellowish tone. Case (c) in LCZ 14 with low plants shows an under-construction area. Case (d) in LCZ 3 shows the photo collected at a location around the downtown square, where the building obstructs human sight within one or two blocks, thus leading to low greenness accessibility. We observe a satisfactory segmentation performance in case (e) of LCZ 11 (i.e., dense trees).

#### 4.2. VGVI distribution

In our study area, we simulate VGVI in more than 235 million observing locations, using the high-performance computer and R programming, running on the Linux operating system.

Fig. 7(a) shows the spatial distribution of VGVI in the study area. The average value of VGVI is 0.49, with a standard deviation of 0.36. The average value reveals that nearly 50 % of greenness visibility appears in Fayetteville, and this percentage is close to the rate of forestland (56 %

in Arkansas (Chhetri and Pelkki, 2022). We also observe that the spatial distribution of VGVI is uneven and heterogeneous. Typically, the highest values occur in parks and natural areas, such as Centennial Park, Kessler Park, and Wilson Springs Nature Preserve. Despite the high greenness visibility in the forest, those areas are hard-to-access places for citizens. Low VGVI values occur in the downtown areas, suggesting low greenness visibility in these areas.

Fig. 7 shows a comparison of VGVI (eye-level view) (Fig. 7(a)) and the distribution of bird-eye greenness, i.e., green and non-green spaces, derived from NDVI (bird-view) in Fayetteville (Fig. 7(b)). In general, VGVI shows a similar distribution to bird-eye greenness. The ubiquitous compact buildings with less greenness in downtown Fayetteville are responsible for the low visible greenness. However, we notice that the visible greenness indicated by VGVI is higher than the bird-eye greenness. Although dense buildings widely exist in the downtown square, the reasonable spatial design of buildings and vegetation can facilitate visible greenness (Xiao et al. (2021)). The zoomed area on the top-left corner presents a community surrounded by high-level vegetation (Fig. 7(b)). We notice that the VGVI for people who live in this community is lower than anticipated due to the sight blocked by dense houses (Fig. 7).

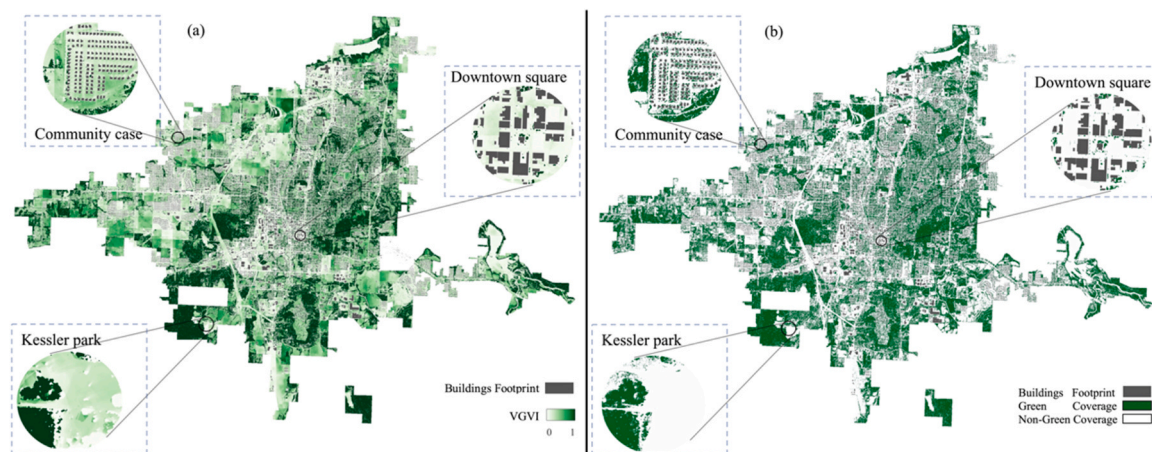


Fig. 7. (a) The distribution of VGVI (eye-level view) in Fayetteville; (b) The distribution of bird-eye greenness derived from remote sensing imagery (bird-view) in Fayetteville.

4.3. The correlation between VGVI and PGVI

Fig. 8 presents the correlation between VGVI and ground-truthing PGVI from the collected panoramas. A significant positive correlation (0.5) based on the TOST equivalence test is observed for all the sampling cases, suggesting the robustness of VGVI in simulating visible greenness in complex urban settings. We notice that the PGVI values are generally below 0.5. Several outliers are plotted in the line of  $y = 1$  (or  $y = 0$ ). Studies have shown that the VGVI model tends to generate value 1 when the observer's location is under trees (Labib et al., 2020, 2021). We assume the value of 0 in VGVI visible green can be attributed to the positioning error. In addition, we observe that more sampling points are distributed above the dashed reference line, meaning that the VGVI tends to be higher than the PGVI. The average VGVI extracted at the corresponding sampling points is 0.22, which is higher than the PGVI of 0.13. Such a phenomenon can be partly explained by the unsatisfactory segmentation of grass, as mentioned in Section 4.1.

When evaluating the results at the LCZ level, we notice that all the LCZs show a highly positive correlation between the VGVI and PGVI, except for the LCZ 3 (i.e., compact lowrise) and LCZ 14 (i.e., low plants). Moreover, based on the marginal density curves, the VGVI demonstrates that the visible greenness in the area of natural land cover types (i.e., LCZ 11–14) is typically higher than the greenness in the area of built

types (i.e., LCZ 3–9). This result is consistent with ground-truthing PGVI, which also partially demonstrates the robustness of the VGVI.

Regarding the insignificant results in LCZ3, the existence of dense buildings can partly explain the insignificant correlation in LCZ 3, as dense buildings pose challenges in extracting VGVI at some sampling points. These points might be close to the facilities or objects like cars that existed when the aircraft with sensors collected the LiDAR point cloud dataset but did not exist when the panoramas were taken. Another potential reason is the sensitivity of resolution in LCZ 3, where dense buildings are widely distributed. A small error in line-of-site can be translated to a large variation of VGVI. In addition, for LCZ 14 (represented by the light green color in Fig. 8), we notice that the VGVI is higher than the PGVI. We believe the grass greenness extraction from panoramas is the leading cause of the mismatch between VGVI and PGVI within LCZ 14 (low plants). Despite the mismatches in these two LCZs, we still believe the VGVI from a 3D urban environment is largely consistent with the PGVI collected from panoramas.

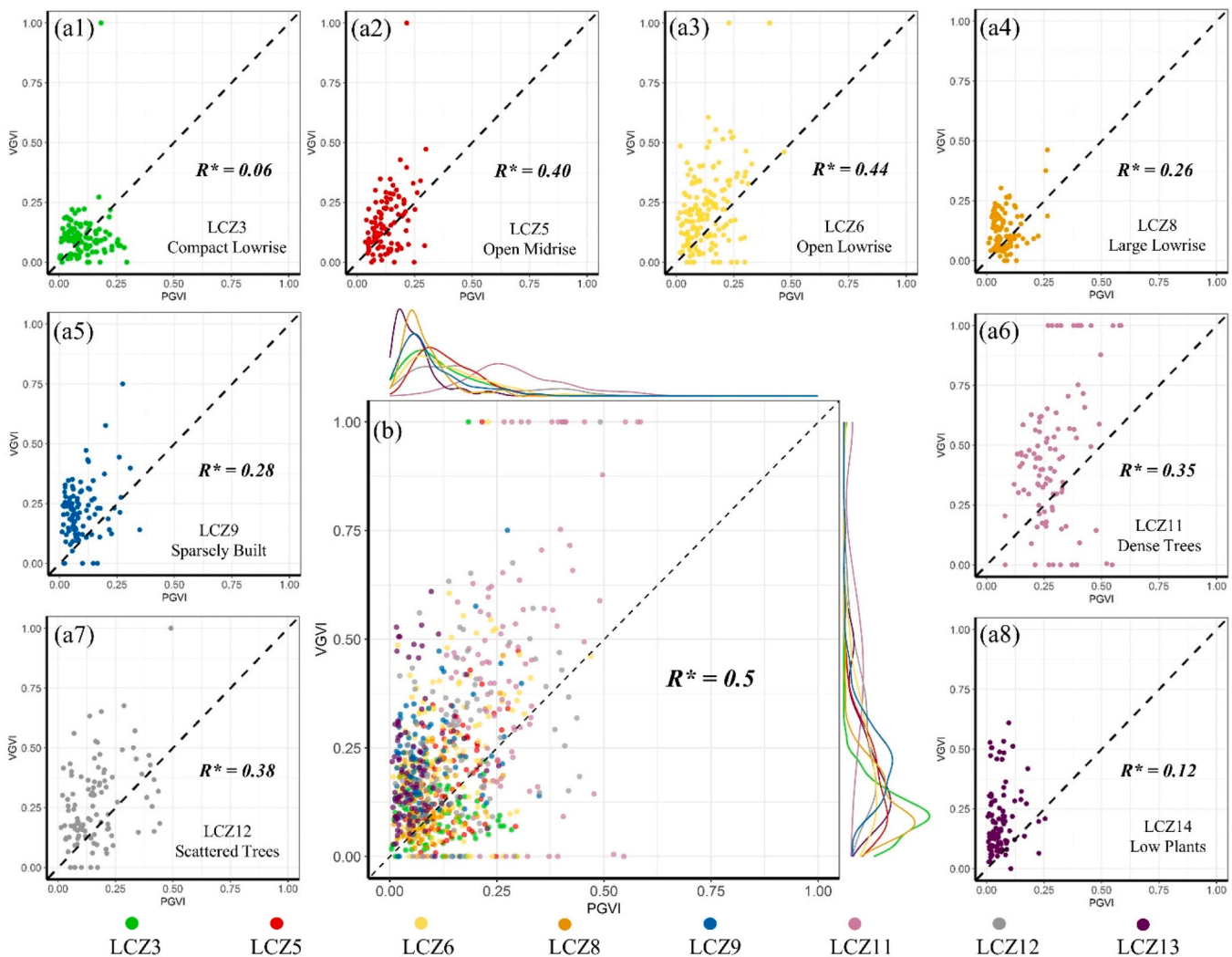


Fig. 8. (a1)–(a8) Scatter plots of simulated VGVI and field-collected PGVI from each LCZ. (b) Scatter plot for all samples from eight LCZs with their marginal density plots, and the dots are with 70 % transparency for better view. R means the correlation coefficient of VGVI and PGVI, and the R with \* represents the significances of TOST equivalent test for the correlation coefficients are at the 0.01 significant level.

## 5. Discussion

### 5.1. The importance of simulated visible greenness and its potential applications

As important agents in urban environments, urban citizens experience greenness with their own eyes. Greenness visibility is strongly associated with positive health outcomes, as documented in the restoration theory by Kaplan (1995). Most existing greenness availability or accessibility studies, however, rely on bird-eye greenness distribution, largely detaching from human experience. Such a limitation has been gradually noted by many scholars, and a significant number of studies have been produced to explore human-perceived greenness in urban environments. In this study, we implemented the VGVI model that simulated visible greenness under a 3D urban context and investigated the performance of VGVI using field-collected panoramas. The results pointed to the promising aspects of visible greenness simulation, as the simulated results present a high consistency compared with ground observations.

In contrast to street view images that primarily focus on the main road, our experiment involves a more flexible and intricate image collection process. We prioritize capturing images in locations where individuals can safely walk or stand, allowing us to gather a broader range of perspectives. From our experiments, we argue that the merits of visible greenness simulation lie in the following aspects. First, its simulative nature allows the acquisition of visible greenness anywhere in a city. Compared to popularly used street-level imagery (e.g., Google, Microsoft, or other crowdsourcing street view platforms) whose coverage issue has been criticized by many, e.g., Quinn and Alvarez León (2019), obtaining visible greenness from a simulation perspective presents great applicable potentials, especially in areas where street views are not available. Second, the adjustable parameters during the simulation offer more flexibility, allowing scholars to examine different scenarios. For example, in our experiment, we used a fixed height of 1.7 m and set the maximum view distance as 550 m, as suggested by Labib et al. (2021). Such a setting can be easily modified in other applications, such as examining the greenness visibility on different floors of high-rise buildings (i.e., adjusting the height parameter) or investigating greenness visibility under different weather conditions (i.e., adjusting the distance parameter). Third, our results suggest that simulated visible greenness and greenness from remote sensing imagery are inconsistent, especially in areas with dense buildings due to the eyesight blocking effects. As Fayetteville, our experimental site, belongs to a mid-size U.S. city, we assume such inconsistency is likely to be exaggerated in bigger cities with denser buildings. We consider simulated visible greenness a promising measure for various domains that favor urban human-perceived greenness exposure, such as environmental psychology, public health (especially mental health), and urban aesthetics. Regarding the urban planning of certain cities, federal or state law imposes maximum height on buildings to protect the city's image and unobstructed views of certain landscapes or civic symbols. The simulated greenness provides essential support for evaluating the impact of building heights and layout on residents' view of greenness and assists planners and stakeholders in proposing strategies to enhance residents' view of nature. Especially for designing and planning new city areas, planners can adopt simulated eye-level greenness to optimize the layout of buildings and greenspace to improve their overall well-being. In addition, we envision a transition of urban greenness inequity studies with the support of visible greenness simulation.

### 5.2. Challenges in simulating visible greenness in complex urban environments

Despite the promising future of visible greenness simulation, several challenges deserve to be mentioned. We notice that such simulation is computationally intensive and demands high performance computer

infrastructure. In our experiment, the VGVI model considers more than 235 million observing locations when establishing the line-of-site calculation in the City of Fayetteville, with a size of 143 km<sup>2</sup>. Even with the support of high-performance computer, obtaining the distribution of simulated visible greenness in this mid-size U.S. city still takes hours. The computational demand is expected to increase exponentially for larger geographic areas. One of the solutions is to divide the entire study area into sub-regions, with each region running its own simulation. Such a strategy allows parallel computing and potentially introduces Graphics Processing Unit for acceleration. However, when simulations are running within regions, errors are unavoidable, especially in areas close to the boundaries of regions (because these boundaries prevent the passing of line-of-sight). The challenge of computational efficiency in visible greenness simulation deserves more attention, and we encourage more efforts toward designing a parallel-computing-enabled simulation environment. In addition, urban environments are dynamic, with fast changes in landscapes, posing additional demand for temporal regularity of the input datasets. Three input datasets are required for the VGVI model, i.e., DEM, DSM, and bird-eye greenness. Ideally, these three datasets need to be collected at the same or close temporal frames to ensure an accurate simulation of visible greenness. Nonetheless, such coordination of the datasets mentioned above is rare, especially with the demand for high-resolution ones.

Furthermore, it is vital to confront the challenge of assessing the generalizability of simulated greenness in case studies beyond Fayetteville. A logical progression for our research is to include locations with a more diverse array of LCZs or different criteria characterizing urban environments. Broadening our research horizons to encompass various geographic locales will enable us to evaluate the extensive applicability and reliability of the simulated greenness methodology. By pursuing further exploration and widening the scope of our research, we can enhance our understanding of VGVI performance within diverse urban contexts, inclusive of regions with higher population densities and complex built environments.

### 5.3. Limitations and future directions

It is important to acknowledge the limitations of this work and provide future research directions. In this study, we evaluated the simulated greenness using field-collected panoramas in Fayetteville. Specifically, we distributed our samples in different LCZs, featured by varying urban landscapes. Concentrating our efforts on Fayetteville allows us to acquire data and insights with wide-ranging applicability and relevance to comparable urban environments. However, considering that Fayetteville is a mid-size U.S. city and does not have certain LCZs exclusive for big cities (e.g., the LCZs of "compact highrise" and "compact midrise"), the performance of VGVI in dense urban environments needs to be further exploited. We also encourage more efforts to investigate the generalizability of simulated greenness in other study cases.

Second, we collected our panoramas during the summer of 2022, when greenness reaches its highest. To make things comparable, the simulated visible greenness relies on the NDVI calculated from NAIP satellite imagery captured in the growing season of 2022. However, we acknowledge that human-perceived greenness changes dramatically given different seasons in a year. The visible greenness in summer and winter usually presents a vast disparity. Although exploring such a disparity is not the focus of this study, we encourage future efforts to explore greenness differences across seasons, an often-overlooked issue in greenness exposure assessment.

Third, we observed some model performance issues during the experiments. For example,

The VGVI model tends to generate value 1 (i.e., 100 % greenness in our field of view) when the observer location is under trees, as the position of the observer falls within the pixel that is labeled green. In real-world scenarios, observers under trees should be able to see other

objects that are not green. Some potential solutions to the model include 1) increasing the resolution of DSM and DEM models and 2) creating different simulating scenarios when observers' locations overlap pixels labeled as green. However, both solutions demand additional computational resources, and future studies need to consider the tradeoff between model performance and computational efficiency.

Finally, we extracted greenness in the panoramas using a pre-trained DeepLab2 model trained on the Cityscapes datasets. Despite DeepLab2 being considered among the state-of-the-art semantic segmentation models, we observed its unsatisfactory performance in grass segmentation (especially when grass presents a yellowish tone), which translates to the higher simulated visible greenness compared to the one captured from panoramas. Considering that segmentation performance comparison is out of the scope of this work, we encourage future efforts to test other image-based greenness segmentation methods, aiming to provide better validation of greenness simulation models.

## 6. Conclusion

This study, conducted in Fayetteville, Arkansas, involves the assessment of the performance of simulated visible greenness (VGVI) by contrasting it with greenness obtained from field-collected panoramas (PVG). By comparing these two metrics, we affirm the robustness and utility of the simulated greenness in quantifying human eye-level visible greenness. This research signifies the inaugural comprehensive evaluation of the robustness of simulated greenness, thereby laying a solid and scientific foundation for future expansive, potentially nationwide, investigations. Our findings indicate a statistically significant correlation, surpassing the 0.01 significance level, between the simulated greenness VGVI and PVGI. When reviewing results at the LCZ level, we observed that most LCZs exhibit a significant positive correlation between the simulated greenness VGVI and PVGI derived from field-collected panoramas. Despite the variation in performance across different LCZs, we posit that VGVI holds substantial promise as a metric across multiple domains that prioritize human-perceived greenness exposure, including environmental psychology, public health (particularly mental health), and urban aesthetics. Given its ability to acquire human-perceived greenness in any urban location, unrestricted by the availability of street view images, we advocate for expanded exploration of VGVI's potential within various urban green space applications.

## CRedit authorship contribution statement

**Jingjing Yan:** Formal analysis, Investigation, Data curation, Writing – original draft, Writing – review & editing, Visualization. **Reza Naghedi:** Validation, Investigation, Writing – original draft. **Xiao Huang:** Data curation, Conceptualization, Methodology, Resources, Writing – original draft, Writing – review & editing, Supervision. **Siqin Wang:** Conceptualization, Supervision, Writing – original draft, Writing – review & editing. **Junyu Lu:** Conceptualization, Supervision, Writing – original draft, Writing – review & editing. **Yang Xu:** Conceptualization, Supervision, Writing – original draft, Writing – review & editing.

## Declaration of Competing Interest

The authors declare no conflict of interests.

## References

Bai, H., Li, Z., Guo, H., Chen, H., Luo, P., 2022. Urban green space planning based on remote sensing and geographic information systems. *Remote Sens.* 14 (17), 4213. <https://doi.org/10.3390/RS14174213>.

Biljecki, F., Ito, K., 2021. Street view imagery in urban analytics and GIS: a review. *Land Urban Plan* 215. <https://doi.org/10.1016/J.LANDURBPLAN.2021.104217>.

Bishop, I.D., 2016. Determination of Thresholds of Visual Impact: The Case of Wind Turbines, 29. SAGE Publications Sage UK, London, England, pp. 707–718. <https://doi.org/10.1068/B12854>.

Boone, C.G., Buckley, G.L., Grove, J.M., Sister, C., 2009. Parks and People: An Environmental Justice Inquiry in Baltimore, Maryland, 99. Taylor & Francis Group, pp. 767–787. <https://doi.org/10.1080/00045600903102949>.

Braun, M., Herold, M., 2004. Mapping imperviousness using NDVI and linear spectral unmixing of ASTER data in the Cologne-Bonn region (Germany).” remote sensing for environmental monitoring, GIS applications, and geology iii, 274–284. SPIE.

Bresenham, J.E., 2010. Algorithm for computer control of a digital plotter. *IBM Syst. J.* 25–30. <https://doi.org/10.1147/SJ.41.0025>.

Brinkmann, S.T., Kremer, D., Walker, B.B., 2022. Modelling eye-level visibility of urban green space: Optimising city-wide point-based viewshed computations through prototyping. *AGILE: GISci. Ser. 3*, 1–7 (Copernicus GmbH).

Census, 2021, (February 9). Bureau, US Census. Retrieved February 13, 2023, from (<https://www.census.gov/>).

Chen, J., Zhou, C., Li, F., 2020. Quantifying the green view indicator for assessing urban greening quality: An analysis based on Internet-crawling street view data. *Ecol. Indic.* 113, 106192.

Chen, Z., Xu, B., Gao, B., 2015. Assessing visual green effects of individual urban trees using airborne Lidar data. *Sci. Total Environ.* 536, 232–244. <https://doi.org/10.1016/J.SCITOTENV.2015.06.142>.

Chhetri, S.G., Pelkki, M., 2022. Current forest management intensity and cost associated with major forestry practices in Arkansas, USA. *J. For. Bus. Res.* 1 (1), 51–74.

City of Fayetteville, Arkansas. (n.d.). Retrieved February 11, 2023, from (<https://www.fayetteville-ar.gov/384/GIS-Interactive-Maps>).

Cordts, M., M. Omran, S. Ramos, T. Rehfeld, M. Enzweiler, R. Benenson, U. Franke, S. Roth, B. Schiele, D.A. R&d, and T.U. Darmstadt. 2016. The Cityscapes Dataset for Semantic Urban Scene Understanding.

Currie, B.A., Bass, B., 2008. Estimates of air pollution mitigation with green plants and green roofs using the UFORE model. *Urban Ecosyst.* 11 (4), 409–422. <https://doi.org/10.1007/S11252-008-0054-Y>.

Daams, M.N., Sijtsma, F.J., Veneri, P., 2019. Mixed monetary and non-monetary valuation of attractive urban green space: a case study using Amsterdam house prices. *Ecol. Econ.* 166, 106430 <https://doi.org/10.1016/J.ECOLECON.2019.106430>.

Demuzere, M., Kittner, J., Martilli, A., Mills, G., Moede, C., Stewart, I.D., van Vliet, J., Bechtel, B., 2022. A global map of local climate zones to support earth system modelling and urban-scale environmental science. *Earth Syst. Sci. Data* 14 (8), 3835–3873. <https://doi.org/10.5194/ESSD-14-3835-2022>.

Dollison, R., Maxwell, J., 2019. The National Map—new data delivery homepage, advanced viewer, lidar visualization. *Fact. Sheet.* <https://doi.org/10.3133/FS20190302>.

Dong, R., Zhang, Y., Zhao, J., 2018. How green are the streets within the sixth ring road of Beijing? An analysis based on tencent street view pictures and the green view index. *Int. J. Environ. Res. Public Health* 15 (7), 1367.

Dzhambov, A.M., Dimitrova, D.D., 2014. Urban green spaces' effectiveness as a psychological buffer for the negative health impact of noise pollution: a systematic review. *Noise Health* 16 (70), 157.

Franco, S.F., Macdonald, J.L., 2018. Measurement and valuation of urban greenness: Remote sensing and hedonic applications to Lisbon, Portugal. *Reg. Sci. Urban Econ.* 72, 156–180.

Gintoli, I., Bellisario, V., Squillacioti, G., Caputo, M., Borraccino, A., Dalmasso, P., Bono, R., Lemma, P., 2020. Urbanization and greenness in HBSC survey: association with life satisfaction and health complaints. *Eur. J. Public Health* 30 (Supplement 5) ckaa166-099. Oxford University Press.

Gunawardena, K.R., Wells, M.J., Kershaw, T., 2017. Utilising green and bluespace to mitigate urban heat island intensity. *Sci. Total Environ.* 584, 1040–1055.

Haaland, C., van den Bosch, C.K., 2015. Challenges and strategies for urban green-space planning in cities undergoing densification: a review. *Urban Urban Green.* 14 (4), 760–771.

Heynen, N., Perkins, H.A., Roy, P., 2006. The political ecology of uneven urban green space: The impact of political economy on race and ethnicity in producing environmental inequality in Milwaukee. *Urban Aff. Rev.* 42 (1), 3–25.

Hu, A. Zhang, J., Kaga, H., 2021. Green View Index Analysis and Optimal Green View Index Path Based on Street View and Deep Learning. arXiv preprint arXiv: 2104.12627.

Jiang, B., Deal, B., Pan, H.Z., Larsen, L., Hsieh, C.H., Chang, C.Y., Sullivan, W.C., 2017. Remotely-sensed imagery vs. eye-level photography: Evaluating associations among measurements of tree cover density. *Land. Urban Plan* 157, 270–281. <https://doi.org/10.1016/J.LANDURBPLAN.2016.07.010>.

Kaplan, S., 1995. The restorative benefits of nature: Toward an integrative framework. *J. Environ. Psychol.* 15 (3), 169–182. [https://doi.org/10.1016/0272-4944\(95\)90001-2](https://doi.org/10.1016/0272-4944(95)90001-2).

de Keijzer, C., Bauwelinck, M., Dadvand, P., 2020. Long-term exposure to residential greenspace and healthy ageing: a systematic review. *Curr. Environ. Health Rep.* 7 (1), 65–88. <https://doi.org/10.1007/S40572-020-00264-7/FIGURES/1>.

Kondo, M.C., Fluehr, J.M., McKeon, T., Branas, C.C., 2018. Urban green space and its impact on human health. *Int. J. Environ. Res. Public Health* 15 (3), 445. <https://doi.org/10.3390/IJERPH15030445>.

Kumsap, C., Borne, F., Moss, D., 2007. The technique of distance decayed visibility for forest landscape visualization. <https://doi.org/10.1080/13658810500104880>, 19 (6): 723–744. Taylor & Francis Group. <https://doi.org/10.1080/13658810500104880>.

Labib, S., Huck, J., Lindley, S., 2020. Greenness visibility using viewshed analysis: A pilot study in Manchester. Proceedings of the 28th Annual Geographical Information Science UK Conference.

- Labib, S.M., Huck, J.J., Lindley, S., 2021. Modelling and mapping eye-level greenness visibility exposure using multi-source data at high spatial resolutions. *Sci. Total Environ.* 755, 143050.
- Lambert, A., Vlaar, J., Herrington, S., Brussoni, M., 2019. What is the relationship between the neighbourhood built environment and time spent in outdoor play? A systematic review. *Int. J. Environ. Res. Public Health* 16 (20), 3840. <https://doi.org/10.3390/IJERPH16203840>.
- Larkin, A., Hystad, P., 2018. Evaluating street view exposure measures of visible green space for health research. *J. Expo. Sci. Environ. Epidemiol.* 29 (4), 447–456, 2018 29:4. (<https://doi.org/10.1038/s41370-018-0017-1>).
- Larkin, A., Hystad, P., 2019. Evaluating street view exposure measures of visible green space for health research. *J. Expo. Sci. Environ. Epidemiol.* 29 (4), 447–456 (Nature Publishing Group).
- Li, X., Ratti, C., 2018. Mapp the spatial distribution of shade provision of street trees in Boston using Google Street View panoramas. *Urban Urban Green.* 31, 109–119. <https://doi.org/10.1016/j.ufug.2018.02.013>.
- Li, X., Zhang, C., Li, W., Ricard, R., Meng, Q., Zhang, W., 2015. Assessing street-level urban greenery using Google Street View and a modified green view index. *Urban Urban Green.* 14 (3), 675–685 (Elsevier).
- Lu, Y., 2019. Using Google Street View to investigate the association between street greenery and physical activity. *Land. Urban Plan* 191, 103435.
- Mara, C.A., Cribbie, R.A., 2012. Paired-samples tests of equivalence. *Commun. Stat. -Simul. Comput.* 41 (10), 1928–1943.
- Meitner, M.J., 2004. Scenic beauty of river views in the Grand Canyon: relating perceptual judgments to locations. *Land. Urban Plan* 68 (1), 3–13. [https://doi.org/10.1016/S0169-2046\(03\)00115-4](https://doi.org/10.1016/S0169-2046(03)00115-4).
- Muhamad Nor, A.N., Abdul Aziz, H., Nawawi, S.A., Muhammad Jamil, R., Abas, M.A., Hambali, K.A., Yusoff, A.H., Ibrahim, N., Rafaai, N.H., Corstanje, R., 2021. Evolution of green space under rapid urban expansion in Southeast Asian cities. *Sustainability* 13 (21), 12024 (MDPI).
- Nutsford, D., Reitsma, F., Pearson, A.L., Kingham, S., 2015. Personalising the viewshed: visibility analysis from the human perspective. *Appl. Geogr.* 62, 1–7. <https://doi.org/10.1016/j.apgeog.2015.04.004>.
- Qian, Y., Zhou, W., Yu, W., Pickett, S.T.A., 2015. Quantifying spatiotemporal pattern of urban greenspace: new insights from high resolution data. *Land. Ecol.* 30 (7), 1165–1173. <https://doi.org/10.1007/S10980-015-0195-3>.
- Qiu, G., Li, H., Zhang, Q., Wan, C., Liang, X., Li, X., 2013. Effects of evapotranspiration on mitigation of urban temperature by vegetation and urban agriculture. *J. Integr. Agric.* 12 (8), 1307–1315.
- Quinn, S., Alvarez León, L., 2019. Every single street? Rethinking full coverage across street-level imagery platforms. *Trans. GIS* 23 (6), 1251–1272. <https://doi.org/10.1111/TGIS.12571>.
- Rzotkiewicz, A., Pearson, A.L., Dougherty, B.V., Shortridge, A., Wilson, N., 2018. Systematic review of the use of Google Street View in health research: major themes, strengths, weaknesses and possibilities for future research. *Health Place* 52, 240–246. <https://doi.org/10.1016/J.HEALTHPLACE.2018.07.001>.
- Sahraoui, Y., Clauzel, C., Foltête, J.C., 2016. Spatial modelling of landscape aesthetic potential in urban-rural fringes. *J. Environ. Manag.* 181, 623–636. <https://doi.org/10.1016/J.JENVMAN.2016.06.031>.
- Shin, J.C., Parab, K.V., An, R., Grigsby-Toussaint, D.S., 2020. Greenspace exposure and sleep: a systematic review. *Environ. Res* 182, 109081. <https://doi.org/10.1016/J.ENVRES.2019.109081>.
- Tabrizian, P., Baran, P.K., van Berkel, D., Mitsova, H., Meentemeyer, R., 2020. Modeling restorative potential of urban environments by coupling viewscape analysis of lidar data with experiments in immersive virtual environments. *Land. Urban Plan* 195. <https://doi.org/10.1016/J.LANDURBPLAN.2019.103704>.
- Thomsen, J.M., Powell, R.B., Monz, C., 2018. A systematic review of the physical and mental health benefits of wildland recreation. *J. Park Recreat Admin.* 123–148. <https://doi.org/10.18666/JPra-2018-V36-11-8095>.
- Twohig-Bennett, C., Jones, A., 2018. The health benefits of the great outdoors: a systematic review and meta-analysis of greenspace exposure and health outcomes. *Environ. Res* 166, 628–637. <https://doi.org/10.1016/J.ENVRES.2018.06.030>.
- Wang, R., Feng, Z., Pearce, J., Yao, Y., Li, X., Liu, Y., 2021. The distribution of greenspace quantity and quality and their association with neighbourhood socioeconomic conditions in Guangzhou, China: a new approach using deep learning method and street view images. *Sustain Cities Soc.* 66, 102664 (Elsevier).
- Wang, W., Lin, Z., Zhang, L., Yu, T., Ciren, P., Zhu, Y., 2019. Building visual green index: a measure of visual green spaces for urban building. *Urban Urban Green.* 40, 335–343.
- Wei, H., Huang, X., Wang, S., Lu, J., Li, Z., Zhu, L., 2022. A data-driven investigation on park visitation and income mixing of visitors in New York City. *Environ. Plan B Urban Anal. City Sci.* [https://doi.org/10.1177/23998083221130708/ASSET/IMAGES/LARGE/10.1177\\_23998083221130708-FIG4.JPEG](https://doi.org/10.1177/23998083221130708/ASSET/IMAGES/LARGE/10.1177_23998083221130708-FIG4.JPEG).
- Williams, E.J., 1959. The comparison of regression variables. *J. R. Stat. Soc.: Ser. B (Methodol.)* 21 (2), 396–399.
- Wolch, J.R., Byrne, J., Newell, J.P., 2014. Urban green space, public health, and environmental justice: the challenge of making cities ‘just green enough. *Land. Urban Plan* 125, 234–244 (Elsevier).
- World bank. Population data. (n.d.). Retrieved January 25, 2023, from (<https://data.worldbank.org/indicator/SP.POP.TOTL>).
- Wu, W., Chen, W.Y., Yun, Y., Wang, F., Gong, Z., 2022. Urban greenness, mixed land-use, and life satisfaction: Evidence from residential locations and workplace settings in Beijing. *Land. Urban Plan* 224, 104428. <https://doi.org/10.1016/J.LANDURBPLAN.2022.104428>.
- Xia, Y., Yabuki, N., Fukuda, T., 2021. Development of a system for assessing the quality of urban street-level greenery using street view images and deep learning. *Urban For. Urban Green.* 59, 126995 <https://doi.org/10.1016/J.UFUG.2021.126995>.
- Xiao, C., Shi, Q., Gu, C.J., 2021. Assessing the spatial distribution pattern of street greenery and its relationship with socioeconomic status and the built environment in Shanghai, China. *Land* 10 (8), 871. <https://doi.org/10.3390/LAND10080871/S1>.
- Yang, B.Y., Zhao, T., Hu, L.X., Browning, M.H.E.M., Heinrich, J., Dharmage, S.C., Jalaludin, B., Knibbs, L.D., Liu, X.X., Luo, Y.N., James, P., Li, S., Huang, W.Z., Chen, G., Zeng, X.W., Hu, L.W., Yu, Y., Dong, G.H., 2021a. Greenspace and human health: an umbrella review. *Innovation* 2 (4), 100164. <https://doi.org/10.1016/j.xinn.2021.100164>.
- Yang, J., Zhao, L., McBride, J., Gong, P., 2009. Can you see green? Assessing the visibility of urban forests in cities. *Land. Urban Plan* 91 (2), 97–104. <https://doi.org/10.1016/J.LANDURBPLAN.2008.12.004>.
- Yang, P.P.J., Putra, S.Y., Li, W., 2007. Viewsphere: a GIS-based 3D visibility analysis for urban design evaluation. *Environ. Plann. B Plann. Des.* 34 (6), 971–992. <https://doi.org/10.1068/B32142>.
- Yin, J., Dong, J., Hamm, N.A.S., Li, Z., Wang, J., Xing, H., Fu, P., 2021. Integrating remote sensing and geospatial big data for urban land use mapping: a review. *Int. J. Appl. Earth Obs. Geoinf.* 103, 102514 <https://doi.org/10.1016/J.JAG.2021.102514>.
- Yu, S., Yu, B., Song, W., Wu, B., Zhou, J., Huang, Y., Wu, J., Zhao, F., Mao, W., 2016. View-based greenery: a three-dimensional assessment of city buildings’ green visibility using Floor Green View Index. *Land. Urban Plan* 152, 13–26. <https://doi.org/10.1016/J.LANDURBPLAN.2016.04.004>.
- Yuan, Y., Huang, F., Lin, F., Zhu, P., Zhu, P., 2021. Green space exposure on mortality and cardiovascular outcomes in older adults: a systematic review and meta-analysis of observational studies. *Aging Clin. Exp. Res.* 33 (7), 1783–1797. <https://doi.org/10.1007/S40520-020-01710-0/FIGURES/3>.
- Zhang, Z., Long, Y., Chen, L., Chen, C., 2021. Assessing personal exposure to urban greenery using wearable cameras and machine learning. *Cities* 109, 103006. <https://doi.org/10.1016/J.CITIES.2020.103006>.